

# FC-Vision: Real-Time Visibility-Aware Replanning for Occlusion-Free Aerial Target Structure Scanning in Unknown Environments

Chen Feng<sup>1,†</sup>, Yang Xu<sup>1</sup>, and Shaojie Shen<sup>1</sup>

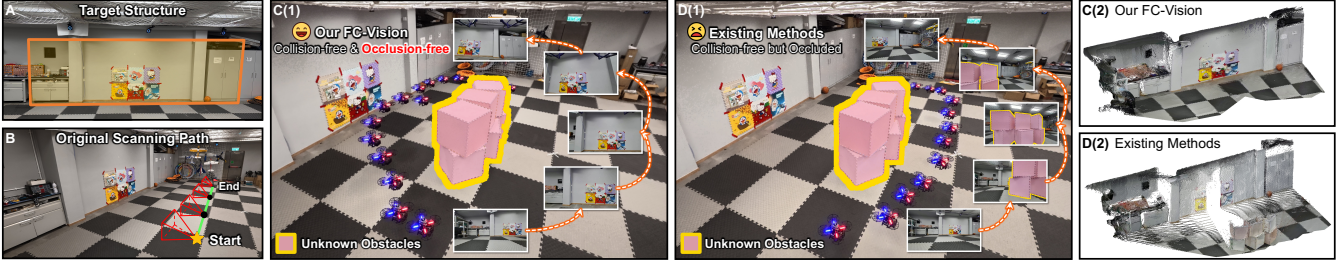


Fig. 1. Teaser. Given a target structure (A) and its nominal scanning plan (B), **FC-Vision** enables real-time replanning to proactively avoid newly emerging unknown obstacles while enforcing collision-free and occlusion-free sensing, thereby preserving the intended coverage and efficiency of the original plan (C). In contrast, existing collision-only replanning fails to prevent FoV blockage, resulting in occluded observations and degraded structural completeness (D).

**Abstract**—Autonomous aerial scanning of target structures is crucial for practical applications, requiring online adaptation to unknown obstacles during flight. Existing methods largely emphasize collision avoidance and efficiency, but overlook occlusion-induced visibility degradation, severely compromising scanning quality. In this study, we propose **FC-Vision**, an on-the-fly visibility-aware replanning framework that proactively and safely prevents target occlusions while preserving the intended coverage and efficiency of the original plan. Our approach explicitly enforces dense surface-visibility constraints to regularize replanning behavior in real-time via an efficient two-level decomposition: occlusion-free viewpoint repair that maintains coverage with minimal deviation from the nominal scan intent, followed by segment-wise clean-sensing connection in 5-DoF space. A plug-in integration strategy is also presented to seamlessly interface **FC-Vision** with existing UAV scanning systems without architectural changes. Comprehensive simulation and real-world evaluations show that **FC-Vision** consistently improves scanning quality under unexpected occluders, delivering a maximum coverage gain of 55.32% and a 73.17% reduction in the occlusion ratio, while achieving real-time performance with a moderate increase in flight time. The source code will be made publicly available.

## I. INTRODUCTION

UNCREWED aerial vehicles (UAVs) increasingly serve to autonomously scan target structures (*e.g.*, interior walls in rooms), supporting infrastructure inspection [1] and spatial reconstruction [2]. In practice, however, scenes are rarely clean or perfectly known: previously unseen objects such as vegetation or temporary equipments may appear unpredictably and continuously reshape feasible flight corridors.

A key challenge is that reactive obstacle clearance alone is insufficient for high-quality scanning. Even when a trajectory is dynamically feasible and safe, newly appeared obstacles may enter the sensor frustum, occluding the target and leaving unobserved surface regions. This causes fragmented coverage and degraded structural completeness, triggering costly re-flights and increasing operational burden. Thus, beyond safety

and efficiency, a practical aerial scanning planner must adapt to unexpected objects in real-time to ensure target visibility: observations should be both complete (high coverage) and clean (suppressing non-target occlusions/clutter in the field of view (FoV)).

Existing studies address parts of this goal but rarely satisfy these requirements simultaneously. Most aerial 3D scanning planners [3]–[6] primarily optimize completeness and efficiency, yet often assume obstacle-free or fully known environments. Online local replanning improves robustness to unforeseen obstacles [7], [8], but such approaches typically follow a navigation-centric flavor [9]–[11] that prioritizes safety and time, treating sensing as a passive byproduct and providing limited safeguards for target visibility. In parallel, visibility objectives are explored in perception-aware planning [12]–[14] and aerial object tracking [15]–[17]. The former category favors informative features for state estimation, yet it does not penalize interference from non-target clutter that harm clean target sensing. The latter imposes sparse line-of-sight (LoS) constraints to keep an object within the FoV, whereas directly transferring such formulations into dense surface coverage is computationally prohibitive at real-time replanning rates. These limitations prevent existing aerial scanning systems from providing explicit guarantees of comprehensive and clean target observations under newly appearing occluders.

To close this gap, we propose **FC-Vision**, a real-time visibility-aware replanning framework tailored for occlusion-free target scanning in unknown environments with safe and efficient flight (Fig.1). Given a target structure and an ongoing scanning path, it proactively avoids both collisions and target occlusions, while respecting the original plan’s intended coverage and efficiency. To achieve low-latency replanning, we decompose this problem into two levels aligned with completeness and cleanliness in target visibility. First, a hybrid sampling-and-optimization procedure generates occlusion-free, safe alternative viewpoints that minimally deviate from the nominal set while maintaining equivalent target coverage, and then computes an intent-consistent visiting order

<sup>1</sup>Department of Electronic and Computer Engineering, The Hong Kong University of Science and Technology, Hong Kong, China.

Email: {cefeng, yxuew, eeshaojie}@ust.hk

† Corresponding Author

by solving a Sequential Ordering Problem to retain efficiency. Second, we connect consecutive viewpoints using our  $\Phi$ -A\* search in 5-DoF representations (3D position plus pitch and yaw), which enables the efficient discrete search in 3D space yet enforces obstacle clearance and FoV-level clean sensing with modest overhead at each expansion, yielding short connectors with continuous clean target observability along the segment. The resulting path is finally converted into a minimum-time trajectory, adhering to safety, feasibility, and complete coverage constraints. Moreover, we develop a plug-in coordination strategy that integrates **FC-Vision** seamlessly into the existing state-of-the-art (SOTA) aerial 3D scanning system without modifying the host architectural stacks.

We evaluate the proposed method against existing SOTA baselines that only consider flight safety but not visibility across diverse challenging real-world and simulated scenarios. **FC-Vision** consistently boosts target visibility while maintaining comparable flight time under real-time computational budgets. In particular, it increases target coverage by up to 55.32% and reduces the occlusion ratio by up to 73.17%. Ablation experiments further validate the effectiveness of our key designs. In summary, the contributions of this paper are:

- 1) A real-time replanning framework that explicitly enforces target visibility amid online-emerging obstacles, yet sustaining safety and efficiency, which is augmented via two novel modules: (i) hybrid sampling-and-optimization viewpoint repair, and (ii)  $\Phi$ -A\* for efficient 5-DoF segment search with joint collision and occlusion avoidance.
- 2) A plug-in system integration that allows existing scanning UAVs to adopt **FC-Vision** in a drop-in manner, without redesigning the underlying pipeline.

3) Extensive real-world and simulation evaluations in unstructured sites that confirm the practicality and performance of our proposed approach. To the best of our knowledge, this is the first work that offers assurance for occlusion-free aerial target structure scanning in unknown environments. The source code of our implementation will be made public.

## II. RELATED WORK

### A. Aerial 3D Scanning Path Planning

A prevalent paradigm for aerial 3D scanning is to (1) select a set of viewpoints that collectively cover the target surface and (2) compute an efficient feasible tour to visit them. Representative works [3], [18], [19] optimize surface-coverage objectives together with viewpoint selection and tour construction. To scale to large and complex scenes, hierarchical planners [4], [6] decompose the target into sub-spaces for efficient global-to-local planning. Later studies [5], [20] further boost viewpoint quality and modeling efficiency via adaptive plane-wise sampling or observability-guided sparse search. Overall, these planners focus on completeness and efficiency but typically assume static, known environments (or pre-mapped obstacles), which reduces reliability when unexpected occluders appear during execution.

To enhance robustness, some systems incorporate online replanning to react to newly observed obstacles and changes in target morphology [7], [8]. Nevertheless, replanning decisions are often driven by collision avoidance and traversal

cost, while target-centric sensing quality (especially occlusion-free, clean observations for dense surface acquisition) is not enforced explicitly, leaving a gap between *flying safely* and *scanning well*.

### B. Visibility-Aware Planning for UAVs

Perception-aware planning couples motion with active vision to improve state estimation, *e.g.*, by steering the drone towards feature-rich regions or informative trajectories that reduce uncertainty [12]–[14]. These methods are effective for robust navigation, but their objectives are predominantly robot-centric and typically do not model how non-target occlusions degrade clean target sensing and dense reconstruction. Visibility constraints are also widely used in aerial tracking, where planners maintain a compact object observable via LoS constraints, 2D visible fans, or differentiable visibility metrics [15]–[17]. These formulations target sparse entities (*e.g.*, a point/box) and are not directly transferable to structure scanning, where dense coverage requires ray-level visibility checks over many surface elements, often significantly expensive for real-time replanning when enforced continuously along a path.

**Our Position.** Different from prior scanning planners and perception-aware navigation or tracking studies, our real-time visibility-aware replanning framework advances existing UAVs to actively and promptly preclude collisions and target occlusions from unknown obstacles, while sustaining information completeness and operational efficiency. This capability enables reliable, occlusion-free scanning of target structures in unknown, cluttered environments via only a single-pass flight.

## III. PROBLEM FORMULATION

We study on-the-fly replanning of an ongoing aerial scanning path  $\bar{\mathcal{P}}$  to handle online-emerging unknown obstacles. A scanning path is an ordered sequence of 5-DoF camera configurations  $q = [\mathbf{p}^\top, \theta, \psi]^\top$  (3D position with pitch and yaw), consisting of viewpoints (for scanning and coverage) and waypoints (for connecting adjacent viewpoints and ensuring feasibility). The camera is modeled as a bounded FoV frustum with sensing range limit  $r_{\max}$ , and an online map  $\hat{\mathcal{O}}$  provides the currently observed environment. Given a target structure,  $\bar{\mathcal{P}}$  defines the intended surface to be covered. We seek a replanned path  $\mathcal{P}$  that preserves this coverage and stays close to  $\bar{\mathcal{P}}$  to retain efficiency, while guaranteeing collision- and occlusion-free execution.

**Unified Joint Problem.** Replanning can be posed as a coupled optimization over the new path  $\mathcal{P}$ , which comprises a set of viewpoints  $\mathcal{V}$  and their connecting segments  $\{\gamma_i\}$ :

$$\begin{aligned} \min_{\mathcal{P}} \quad & \mathcal{J}_{\text{dev}}(\mathcal{P}, \bar{\mathcal{P}}) + \text{Len}(\mathcal{P}) \\ \text{s.t.} \quad & \mathcal{C}(\mathcal{P}) \geq \mathcal{C}(\bar{\mathcal{P}}), \text{dist}(\mathcal{P}, \hat{\mathcal{O}}) \geq d_{\min}, \text{Occ}(\mathcal{P}, \hat{\mathcal{O}}) = 0, \end{aligned} \quad (1)$$

where  $\mathcal{J}_{\text{dev}}$  penalizes deviation from the nominal scan intent (mainly on viewpoints),  $\mathcal{C}(\cdot)$  measures target coverage contributed by viewpoint FoVs, and  $\text{Occ}(\cdot)$  indicates FoV-level non-target occlusion. Solving Eq.(1) under strict latency is difficult because (i) visibility depends on discrete ray-geometry interactions over common 3D representations (point clouds, meshes, occupancy), yielding non-smooth and discontinuous constraints; (ii) coverage preservation couples

viewpoints and their order through a set-coverage/tour-style combinatorial structure; and (iii) observation cleanliness must hold continuously along each segment whenever online map updates. Together, these factors make the problem highly non-convex, rendering it impractical to optimize at real-time rates. **Two-Level Decomposition.** To enable low-latency replanning, we approximate Eq.(1) by a two-level decomposition in accordance with two visibility criteria: completeness (comprehensive coverage) and cleanliness (fully occlusion-free FoV).

a) *Level-I: Viewpoint update under coverage and occlusion constraints:* We first compute a safe viewpoint set  $\mathcal{V} = \{\mathbf{v}_k\}_{k=1}^K$  and a visiting order  $\pi$  that minimally deviates from the reference set  $\bar{\mathcal{V}}$ , while preserving nominal coverage and ensuring occlusion-free sensing at viewpoints:

$$\begin{aligned} \min_{\mathcal{V}, \pi} \quad & \mathcal{D}_{\text{set}}(\mathcal{V}, \bar{\mathcal{V}}) + \sum_{k=1}^{K-1} c(\mathbf{v}_{\pi_k}, \mathbf{v}_{\pi_{k+1}}) \\ \text{s.t.} \quad & \mathcal{C}(\mathcal{V}) \geq \mathcal{C}(\bar{\mathcal{P}}), \mathbf{v} \in \mathcal{V}_{\text{free}}(\hat{\mathcal{O}}), \text{Occ}(\mathbf{v}, \hat{\mathcal{O}}) = 0, \end{aligned} \quad (2)$$

where  $\mathcal{D}_{\text{set}}$  measures set-to-set discrepancy (e.g., Chamfer distance),  $\mathcal{V}_{\text{free}}(\hat{\mathcal{O}})$  enforces viewpoint safety with clearance, and  $c(\cdot, \cdot)$  is the travel cost for tour optimization.

b) *Level-II: Segment-wise clean-sensing connection in 5-DoF space.:* Given the ordered viewpoints, we connect each consecutive pair with a shortest 5-DoF segment that remains safe and occlusion-free throughout:

$$\begin{aligned} \min_{\gamma_k} \quad & \text{Len}(\gamma_k) \\ \text{s.t.} \quad & \text{dist}(\gamma_k, \hat{\mathcal{O}}) \geq d_{\min}, \text{Occ}(\gamma_k, \hat{\mathcal{O}}) = 0. \end{aligned} \quad (3)$$

#### IV. FRAMEWORK OVERVIEW

Building on the two-level decomposition in Sec.III, we develop **FC-Vision** as a low-latency replanning framework that locally repairs an ongoing scan under online-emerging obstacles (Fig.2). Starting from the target structure and the current scanning path  $\bar{\mathcal{P}}$ , we derive the intended surface set  $\mathcal{S}$  by aggregating the FoVs of its viewpoints. With the updated online map  $\hat{\mathcal{O}}$ , **FC-Vision** first repairs the viewpoint set to preserve coverage of  $\mathcal{S}$  while enforcing per-viewpoint clearance and occlusion-free observation, and then reorders the repaired viewpoints to minimize travel cost while respecting the nominal scan progression (Sec.V-A). It next bridges each consecutive viewpoint pair via a short, collision-free and clean-sensing 5-DoF connector, discretizes the connector into executable waypoints, and assembles the replanned path  $\mathcal{P}$ , which is subsequently converted into a feasible trajectory for execution (Sec.V-B). Finally, **FC-Vision** is deployed as a plug-in replanning layer that interfaces with existing UAV scanning systems: the upstream planner provides  $\bar{\mathcal{P}}$ , while our module performs event-triggered local repair when newly observed obstacles threaten either safety or clean sensing, without altering the host pipeline (Sec.V-C).

#### V. METHODOLOGY

##### A. Occlusion-free Viewpoint Repair with Coverage Preservation and Tour Reordering

To begin, we detect nominal viewpoints whose intended observations become contaminated by newly sensed non-target

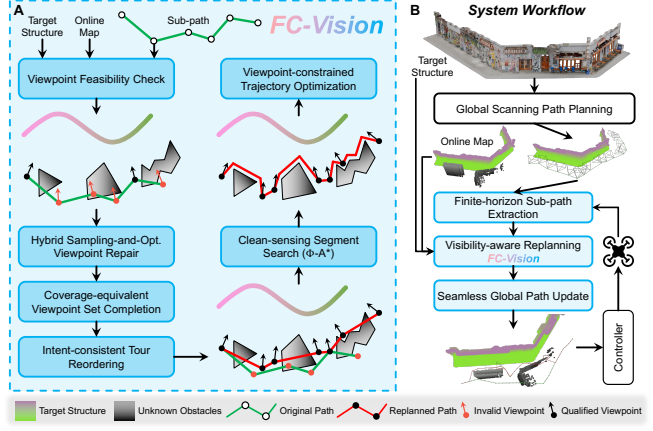


Fig. 2. (A) Framework overview **FC-Vision**. (B) Workflow of aerial scanning system boosted by our visibility-aware replanning (Blue).

obstacles. The target surface is discretized into elements  $\mathcal{S} = \{\mathbf{e}_j\}_{j=1}^N$ . From the nominal scan  $\bar{\mathcal{P}}$ , we extract its viewpoint set  $\bar{\mathcal{V}} = \{\bar{\mathbf{v}}_i\}$ . For each  $\bar{\mathbf{v}}_i$ , we collect its intended subset  $\mathcal{S}_i$  (elements inside its FoV) and raycast each  $\mathbf{e} \in \mathcal{S}_i$  against the online map  $\hat{\mathcal{O}}$ . A viewpoint is “qualified” if it satisfies safety margin and occlusion-free sensing on  $\mathcal{S}_i$ ; otherwise it is marked “invalid”, which is stored  $\bar{\mathcal{V}}_{\text{qual}}$  and repair  $\bar{\mathcal{V}}_{\text{inv}}$ , respectively. Jointly optimizing 5-DoF viewpoint poses and a visiting order forms a non-convex Mixed-Integer Nonlinear Programming (MINLP) with map-dependent visibility constraints, hence we decouple it into (i) viewpoint repair and (ii) tour reordering.

**Hybrid Sampling-and-Optimization Viewpoint Repair.** Direct pose optimization is robust but too slow online due to dense ray-geometry evaluations, whereas sampling-based fashion suffers from a severe quality-density trade-off and unstable solutions under sparse sampling. We thus take the best of both: FoV-truncated sampling proposes a small candidate set, and an analytic refinement rapidly improves each candidate under exact frustum constraints (Fig.3).

(1) *FoV-truncated spherical sampling.* We precompute a reusable direction template in a canonical frame (origin-centered, forward  $+x$  axis) and sample angular offsets  $(\theta, \psi)$  limited by the horizontal ( $\alpha_h$ ) and vertical ( $\alpha_v$ ) angles of FoV:

$$\theta = n\Delta\theta \in (-\alpha_v, \alpha_v), \psi = m\Delta\psi \in (-\alpha_h, \alpha_h). \quad (4)$$

Each sample maps to a unit ray direction  $\mathbf{u}(\theta, \psi) = [\cos\psi \cos\theta, \cos\psi \sin\theta, \sin\psi]^T$  that is generated once and reused. For an invalid viewpoint  $\bar{\mathbf{v}}$ , we compute an anchor point  $\mathbf{m}(\bar{\mathbf{v}})$  (geometric median of its intended subset) and instantiate candidates on a sphere of radius  $r_{\max}$ :

$$\mathbf{p}_i = \mathbf{m}(\bar{\mathbf{v}}) + r_{\max} \mathbf{R}(\bar{\mathbf{v}}) \mathbf{u}(\theta_i, \psi_i), \quad (5)$$

where  $\mathbf{R}(\bar{\mathbf{v}})$  rotates the canonical  $+x$  axis to its viewing direction. This canonical-template reuse avoids per-viewpoint template regeneration and stabilizes candidate quality.

(2) *Analytic position refinement along the viewing ray.* For a sampled candidate with fixed  $(\theta_i, \psi_i)$  and viewing direction  $\mathbf{d}$ , we optimize only its camera center by translating along  $\mathbf{d}$ :

$$\mathbf{p}(s) = \mathbf{p}_i + s\mathbf{d}, \quad s \geq 0. \quad (6)$$

The FoV frustum in world coordinates is modeled as the intersection of five half-spaces  $\mathcal{M} = \{\text{Left, Right, Up, Down, Far}\}$ :

$$\mathcal{F}(\mathbf{p}, \theta_i, \psi_i) = \bigcap_{m \in \mathcal{M}} \{\mathbf{x} \in \mathbb{R}^3 \mid \mathbf{n}_m^\top \mathbf{x} + h_m(\mathbf{p}, \theta_i, \psi_i) \leq 0\}, \quad (7)$$

and the offsets vary affinely with  $s$ :

$$h_m^s = h_m(\mathbf{p}_i, \theta_i, \psi_i) - s \mathbf{n}_m^\top \mathbf{d}. \quad (8)$$

We first remove self-occluded target elements under  $(\theta_i, \psi_i)$  to obtain  $\mathcal{S}_i^{\text{vis}}$ . Coverage at offset  $s$  is defined as the fraction of  $\mathcal{S}_i^{\text{vis}}$  inside the shifted FoV:

$$\text{Cov}(s) = \frac{1}{|\mathcal{S}_i^{\text{vis}}|} \sum_{\mathbf{e} \in \mathcal{S}_i^{\text{vis}}} \mathbf{1}[\forall m \in \mathcal{M} : \mathbf{n}_m^\top \mathbf{e} + h_m^s \leq 0]. \quad (9)$$

To enforce clean sensing, let  $\mathcal{O}_{\text{in}}$  be obstacle samples inside  $\mathcal{F}(\mathbf{p}_i, \theta_i, \psi_i)$  at  $s = 0$  and define  $\kappa_m(\mathbf{o}) \triangleq \mathbf{n}_m^\top \mathbf{o} + h_m(\mathbf{p}_i, \theta_i, \psi_i)$ . The minimum shift to expel  $\mathbf{o}$  with safety margin  $d_{\min}$  to impose collision avoidance has a closed form:

$$s_{\text{out}}(\mathbf{o}) = \min_{m: \mathbf{n}_m^\top \mathbf{d} < 0} \frac{d_{\min} - \kappa_m(\mathbf{o})}{-\mathbf{n}_m^\top \mathbf{d}}, \quad s_{\text{lb}} = \max_{\mathbf{o} \in \mathcal{O}_{\text{in}}} s_{\text{out}}(\mathbf{o}), \quad (10)$$

so any  $s \geq s_{\text{lb}}$  guarantees an obstacle-free FoV for this ray direction with safe clearance. We then choose  $s$  to maximize coverage under this feasibility bound:

$$s^* \in \arg \max_{s \geq s_{\text{lb}}} \text{Cov}(s). \quad (11)$$

Each element  $\mathbf{e} \in \mathcal{S}_i^{\text{vis}}$  induces a 1D bound interval  $I(\mathbf{e}) = [\ell(\mathbf{e}), u(\mathbf{e})]$  from the five affine inequalities  $\mathbf{n}_m^\top \mathbf{e} + h_m(\mathbf{p}_i, \theta_i, \psi_i) - s \mathbf{n}_m^\top \mathbf{d} \leq 0$ , hence Eq.(11) reduces to selecting  $s$  that maximizes interval overlap:

$$s^* \in \arg \max_{s \geq s_{\text{lb}}} \sum_{\mathbf{e} \in \mathcal{S}_i^{\text{vis}}} \mathbf{1}[s \in I(\mathbf{e})], \quad (12)$$

solvable in  $O(|\mathcal{S}_i^{\text{vis}}| \log |\mathcal{S}_i^{\text{vis}}|)$  via a sweep over interval endpoints [21]. The refined candidate is  $\mathbf{v}^* = [\mathbf{p}(s^*)^\top, \theta_i, \psi_i]^\top$ .

(3) *Local pitch and yaw bisection refinement.* After fixing  $\mathbf{p}^* = \mathbf{p}(s^*)$ , we refine  $(\theta_i, \psi_i)$  to further improve visible target coverage within tight admissible bounds derived from the closest obstacle bearings. Let  $\mathcal{O}_{\text{nb}}$  be obstacle samples near the current frustum boundary at  $\mathbf{p}^*$ . Transform a sample  $\mathbf{o} \in \mathcal{O}_{\text{nb}}$  into the camera frame under  $(\theta_i, \psi_i)$ :  $\mathbf{r}(\mathbf{o}) = \mathbf{R}(\theta_i, \psi_i)^\top (\mathbf{o} - \mathbf{p}^*) = [x, y, z]^\top$ , and define its horizontal/vertical bearings  $\beta_h(\mathbf{o}) = \arctan(y, x)$ ,  $\beta_v(\mathbf{o}) = \arctan(z, x)$ . Since the FoV limits correspond to  $|\beta_h| \leq \alpha_h/2$  and  $|\beta_v| \leq \alpha_v/2$ , the maximum orientation perturbations before  $\mathbf{o}$  hits the left/right or up/down plane are given by the angular margins

$$\eta_h = \min_{\mathbf{o} \in \mathcal{O}_{\text{nb}}} \left( |\beta_h(\mathbf{o})| - \frac{\alpha_h}{2} \right), \quad \eta_v = \min_{\mathbf{o} \in \mathcal{O}_{\text{nb}}} \left( |\beta_v(\mathbf{o})| - \frac{\alpha_v}{2} \right), \quad (13)$$

yielding  $\psi \in [\psi_i - \eta_h, \psi_i + \eta_h]$  and  $\theta \in [\theta_i - \eta_v, \theta_i + \eta_v]$ . Within these bounds, we adopt bisection in two dimensions to rapidly find a desired look-at orientation  $(\theta_{\text{des}}, \psi_{\text{des}})$  that maximizes coverage and does not violate the occlusion-free constraint, producing the final repaired viewpoint  $\mathbf{v}^* = [\mathbf{p}(s^*)^\top, \theta^*, \psi^*]^\top$ .

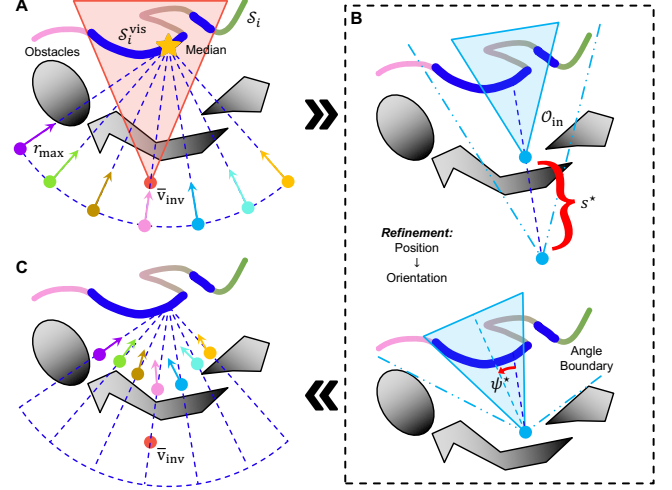


Fig. 3. Illustration of hybrid sampling-and-optimization viewpoint repair. (A) FoV-truncated spherical sampling. (B) Analytic position optimization and local orientation refinement. (C) Repaired collision-free and occlusion-free sampling candidates.

**Coverage-equivalent Viewpoint Set Completion.** For each invalid viewpoint  $\bar{\mathbf{v}}_i$ , Steps (1)-(3) yield a candidate pool  $\mathcal{Q}_i$  (collision-free, clean FoV). Jointly selecting a repaired set from  $\mathcal{Q} = \cup_i \mathcal{Q}_i$  to preserve global coverage is set-cover-style NP-hard [22], so we utilize a greedy procedure. We first pick one replacement per  $\bar{\mathbf{v}}_i$ :

$$\mathbf{v}_i^* = \arg \max_{\mathbf{v} \in \mathcal{Q}_i} \frac{|\text{Cov}(\mathbf{v}) \cap \mathcal{S}_i|}{|\mathcal{S}_i|} - \lambda_d \|\mathbf{p}(\mathbf{v}) - \bar{\mathbf{p}}_i\|_2. \quad (14)$$

Replacing all invalid viewpoints yields an initial repaired set  $\mathcal{V}_0$ , and then a small residual uncovered subset may remain:  $\mathcal{U} = \mathcal{S} \setminus \text{Cov}(\mathcal{V}_0)$ . We optionally add a few auxiliary viewpoints to cover  $\mathcal{U}$  while staying close to the current set  $\mathcal{V}_{\text{cur}} = \mathcal{V}_0 \cup \bar{\mathcal{V}}_{\text{qual}}$ . Let  $\Delta(\mathbf{v}) = \text{Cov}(\mathbf{v}) \cap \mathcal{U}$  and  $d_{\text{nn}}(\mathbf{v}, \mathcal{V}_{\text{cur}}) = \min_{\mathbf{u} \in \mathcal{V}_{\text{cur}}} \|\mathbf{p}(\mathbf{v}) - \mathbf{p}(\mathbf{u})\|_2$ . We iteratively select

$$\mathbf{v}^* = \arg \max_{\mathbf{v} \in \mathcal{Q}} \frac{|\Delta(\mathbf{v})|}{|\mathcal{U}|} - \lambda_d d_{\text{nn}}(\mathbf{v}, \mathcal{V}_{\text{cur}}), \quad (15)$$

update  $\mathcal{V}_{\text{cur}} \leftarrow \mathcal{V}_{\text{cur}} \cup \{\mathbf{v}^*\}$  and  $\mathcal{U} \leftarrow \mathcal{U} \setminus \Delta(\mathbf{v}^*)$  until  $\mathcal{U}$  is fully covered by all viewpoints in  $\mathcal{V}_{\text{cur}}$ .

**Intent-consistent Tour Reordering.** After viewpoint repair, we compute an efficient visiting order to retain efficiency but avoid drastically changing the original scan progression. Consequently, we explicitly preserve the relative order of the originally qualified viewpoints  $\bar{\mathcal{V}}_{\text{qual}} = \{\bar{\mathbf{v}}_0, \dots, \bar{\mathbf{v}}_{M-1}\}$  as precedence anchors, and only allow newly repaired or added viewpoints to be inserted between them. This can be formulated as a Sequential Ordering Problem (SOP) [23]:

$$\min_{\pi} \sum_k c(\mathbf{v}_{\pi_k}, \mathbf{v}_{\pi_{k+1}}) \quad \text{s.t. } \bar{\mathbf{v}}_0 \prec \bar{\mathbf{v}}_1 \prec \dots \prec \bar{\mathbf{v}}_{M-1}, \quad (16)$$

where  $c(\cdot, \cdot)$  is Euclidean travel cost. The precedence constraints encode the nominal scan progression and prevent large-scale backtracking, while SOP minimizes traversal by inserting repaired viewpoints.

#### B. Clean-sensing Segment Search and Trajectory Generation

Given the viewpoint set  $\mathcal{V}_{\text{cur}} = \{\mathbf{v}_{\pi_0}, \dots, \mathbf{v}_{\pi_{K-1}}\}$  from Level-I, we bridge each consecutive pair  $\mathbf{v}_a = \mathbf{v}_{\pi_k}$  and

$\mathbf{v}_b = \mathbf{v}_{\pi_{k+1}}$  by a short connector that is both collision-free and clean-sensing along the entire segment. This step is essential: viewpoint-level cleanliness alone is insufficient since a collision-free connector may still pass through intermediate configurations whose FoV is contaminated by online-emerging occluders, breaking the visibility cleanliness guarantee. The main challenge is that dense ray-level visibility checking is prohibitively expensive, and a direct search in discretized 5-DoF space quickly becomes intractable. To address this, we propose a novel  $\Phi$ -A\* search that efficiently finds high-quality clean-sensing segments under critical latency constraints, as illustrated in Algo.1.

Our key idea is to keep the discrete search in 3D space (camera positions) while enforcing 5-DoF clean-sensing feasibility at each expansion through an efficient lifting mapping function  $\Phi$ . Specifically, we run a weighted A\* on a 3D voxel grid of camera position  $\mathbf{p}$ :

$$f(\mathbf{p}) = g(\mathbf{p}) + \lambda_{\text{heu}} \|\mathbf{p} - \mathbf{p}_b\|_2, \quad (17)$$

where  $g$  accumulates Euclidean step costs and  $\lambda_{\text{heu}}$  biases the search towards the goal. For each expanded  $\mathbf{p}$ , we lift it to a 5-DoF camera configuration  $q = [\mathbf{p}^\top, \theta, \psi]^\top$  via

$$\begin{aligned} (\theta, \psi) &= \Phi(\mathbf{p}) = (1 - \rho)(\theta_a, \psi_a) + \rho(\theta_b, \psi_b) \\ \rho &= \frac{\|\mathbf{p} - \mathbf{p}_a\|_2}{\|\mathbf{p} - \mathbf{p}_a\|_2 + \|\mathbf{p} - \mathbf{p}_b\|_2}. \end{aligned} \quad (18)$$

This *lifted-state* design prevents the combinatorial explosion of 5D grid search, yet still validates collision clearance and FoV cleanliness in the full 5-DoF configuration at every node.

**Bounded Constant-time Occlusion-aware Attitude Correction.** A distinctive advantage of  $\Phi$ -A\* is that a visibility failure at a 3D node does *not* necessarily require changing the node to avoid spatial detours and extra branching. Instead, when the lifted configuration  $q$  is occluded, we locally correct  $(\theta, \psi)$  under the frustum half-space representation in Eq.(7). To bound the computational overhead, we query only a constant-size local voxel set  $\mathcal{O}_{\text{loc}}(q)$  and denote  $\mathbf{o}^*$  as the closest sample to the most violated side plane. The admissible pitch/yaw margins before  $\mathbf{o}^*$  enters the FoV follow Eq.(13), with which we solve a 2D minimum-perturbation adjustment for clean sensing:

$$\begin{aligned} (\Delta\theta^*, \Delta\psi^*) &= \arg \min_{\Delta\theta, \Delta\psi} |\Delta\theta| + |\Delta\psi| \\ \text{s.t. } \text{Occ}\left([\mathbf{p}^\top, \theta + \Delta\theta^*, \psi + \Delta\psi^*]^\top, \hat{\mathcal{O}}\right) &= 0, \end{aligned} \quad (19)$$

Since  $\mathbf{o}^*$  induces a single-boundary feasibility transition with respect to the pitch and yaw axes, the constraint becomes effectively monotone along the interpolation direction, enabling a short bisection to locate the smallest feasible correction. This procedure is constant-time per expansion:  $|\mathcal{O}_{\text{loc}}(q)|$  is bounded by the local voxel query, and the bisection runs for at most a fixed  $N_{\text{bis}}$  iterations on two axes. The repaired  $(\theta, \psi)$  is stored as a node annotation for path reconstruction, substantially improving the probability of finding short clean-sensing connectors under strict latency.

**Visibility Cache for Amortized Acceleration.** During node expansions, many lifted configurations are repeatedly

---

**Algorithm 1:**  $\Phi$ -A\*: Clean-sensing Segment Search

---

```

Input: Start/end viewpoints  $\mathbf{v}_a, \mathbf{v}_b$ ; Online map  $\hat{\mathcal{O}}$ ; Search step  $\Delta_p$ ; Heuristic weight  $\lambda_{\text{heu}}$ ; Clearance  $d_{\min}$ 
Output: Clean-sensing connector  $\gamma_k$  (or FAIL)
1 Initialization: Open set  $\mathcal{Y} \leftarrow \{\mathbf{p}_a\}$ ;  $g(\mathbf{p}_a) \leftarrow 0$ ; Parent map  $\text{par}(\cdot)$ ; Attitude annotation  $\text{att}(\mathbf{p}_a) \leftarrow (\theta_a, \psi_a)$ ; Visibility cache  $\text{cache} \leftarrow \emptyset$ ;
2 while  $\mathcal{Y} \neq \emptyset$  and within time budget do // Eq.(17)
3   Pop  $\mathbf{p}$  with the smallest  $f(\mathbf{p})$  in  $\mathcal{Y}$  ;
4   if  $\|\mathbf{p} - \mathbf{p}_b\|_2 == 0$  then
5     Backtrack 3D chain  $\{\mathbf{p}_t\}$  using  $\text{par}(\cdot)$  and assign  $(\theta_t, \psi_t) = \text{att}(\mathbf{p}_t)$ ;
6     return  $\gamma_k = \{[\mathbf{p}_t^\top, \theta_t, \psi_t]^\top\}$ ;
7   foreach neighbor  $\mathbf{p}' \in \mathcal{N}(\mathbf{p}; \Delta_p)$  do
8     if  $\text{dist}(\mathbf{p}', \hat{\mathcal{O}}) < d_{\min}$  then
9       continue;
10     $(\theta, \psi) \leftarrow \Phi(\mathbf{p}')$  ; // Eq.(18)
11     $q \leftarrow ([\mathbf{p}']^\top, \theta, \psi)^\top$  ;
12    if  $\text{cache}[\tau(q)] \neq \text{true}$  then
13      if  $\text{FAIL} \leftarrow \text{VisCleanTest}(q, \hat{\mathcal{O}})$  then
14        if  $(\theta, \psi) \leftarrow \text{AttCorrect}(q, \hat{\mathcal{O}})$  then
15           $q \leftarrow ([\mathbf{p}']^\top, \theta, \psi)^\top$  ;
16           $\text{cache}[\tau(q)] \leftarrow \text{true}$  ;
17        else
18          continue ;
19     $g_c \leftarrow g(\mathbf{p}) + \lambda_{\text{heu}} \|\mathbf{p}' - \mathbf{p}\|_2$  ;
20    if  $g_c < g(\mathbf{p}')$  then
21       $g(\mathbf{p}') \leftarrow g_c$ ;  $\text{par}(\mathbf{p}') \leftarrow \mathbf{p}$ ;  $\text{att}(\mathbf{p}') \leftarrow (\theta, \psi)$  ;
22      Push or update  $\mathbf{p}'$  in  $\mathcal{Y}$  with key  $f(\mathbf{p}')$  ;
23 return FAIL;

```

---

queried with highly similar  $(\mathbf{p}, \theta, \psi)$ . We therefore memoize the clean-sensing result using a quantized key  $\tau(q) = (\lfloor \mathbf{p}/\Delta_p \rfloor, \lfloor \theta/\Delta_\theta \rfloor, \lfloor \psi/\Delta_\psi \rfloor)$ . Cache hits bypass FoV testing entirely, while cache misses trigger one evaluation and store the result. This amortizes the cost of visibility checks and substantially improves replanning throughput without weakening the cleanliness constraint.

**Trajectory Generation.** Once all segments are found, we concatenate them with  $\mathcal{V}_{\text{cur}}$  to assemble the full repaired path. This sequence is then converted into a minimum-time and dynamically feasible trajectory using the viewpoint-constrained trajectory optimization [24] satisfying high smoothness, obstacle avoidance, and coverage completeness.

### C. Efficient Plug-in System Integration

A practical challenge for visibility-aware replanning is deployability: most aerial scanning systems already have a mature stack (global view planning  $\rightarrow$  trajectory optimization  $\rightarrow$  control), and redesigning the whole pipeline is typically costly. **FC-Vision** is therefore devised as a plug-in layer that upgrades existing systems to be occlusion-aware through a minimal interface while reusing the host execution modules. We treat the nominal scanning path  $\bar{\mathcal{P}}$  produced by any upstream planner as a reference intent: its ordered sequence of 5-DoF viewpoints defines the intended target subset  $\mathcal{S}$  and scan progression. Our algorithm takes  $(\bar{\mathcal{P}}, \hat{\mathcal{O}})$  as input and returns a repaired path  $\mathcal{P}$  in the same representation, so that downstream components remain unchanged. This makes

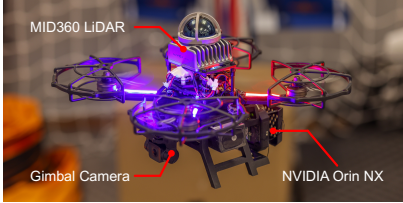


Fig. 4. The UAV platform used in real-world scanning flight tests.

the integration planner-agnostic and allows **FC-Vision** to be attached to a wide range of scanning stacks.

To meet strict latency, we avoid global re-optimization and operate in a receding-horizon fashion. At each replanning call, we extract a local sub-path  $\bar{\mathcal{P}}_{[i_s, i_e]}$  by accumulating arc-length up to a fixed horizon  $\mathcal{H}$  ahead of the current execution. Our replanning framework then repairs only this window to satisfy collision- and occlusion-free throughout, and we seamlessly splice it back to form the updated scan plan:

$$\mathcal{P}_{\text{update}} \leftarrow \bar{\mathcal{P}}_{[0, i_s]} \oplus \bar{\mathcal{P}}_{[i_s, i_e]}^{\text{replan}} \oplus \bar{\mathcal{P}}_{(i_e, |\bar{\mathcal{P}}|]}. \quad (20)$$

This preserves the upstream scan intent outside the affected region and prevents unnecessary tour disruption, while reacting promptly to local changes. The plug-in is invoked in an event-driven manner whenever newly observed obstacles would violate clearance or clean sensing along the current path, and is complemented by a lightweight periodic refresh to remain synchronized with the evolving online map. Importantly, replanning runs with a strict time budget and returns the best feasible repair found within the budget, ensuring responsiveness in closed-loop flight. By isolating visibility reasoning into a fast local repair layer, **FC-Vision** enables drop-in adoption by existing scanners, retaining their mature planning stacks while adding real-time occlusion-aware corrections when the environment changes.

## VI. EXPERIMENTS

### A. Experimental Setup

**Implementation Details.** The UAV carries a 3D LiDAR for online mapping and unexpected-obstacle detection, and a gimbal-mounted RGB camera for flexible surface scanning. For real-world tests, we customize a quadrotor platform (Fig.4) where the LiDAR and gimbal camera are specified as a Livox MID360 and a SIYI A2 Mini, with all modules running onboard on an NVIDIA Orin NX edge computer. In simulation, AirSim [25] serves as the physics simulator, and the same pipeline is deployed on a desktop workstation (Intel Core i9-12900K CPU). To ensure consistent evaluation, we align platform and sensor parameters across both simulation and real flights: the UAV is modeled with a radius of 0.2 m; the LiDAR measurement range is capped at 15 m; the camera has a FoV of  $[\alpha_h = 80^\circ, \alpha_v = 65^\circ]$  with the pitch limited to  $[-80^\circ, +30^\circ]$ ; and its effective sensing range is constrained to  $r_{\text{max}} = 7$  m. Building on the above configuration, we next detail the algorithmic implementation used throughout all experiments. The online map  $\hat{\mathcal{O}}$  is represented by voxels at a resolution of 0.1 m. In Sec.V-A, the safety margin  $d_{\text{min}}$  equals the UAV radius, and  $\lambda_d = 5.0$  is adopted for viewpoint selection. For the  $\Phi\text{-A}^*$  search in Sec.V-B, we set the search step  $\Delta_p = 0.1$  m, heuristic weight  $\lambda_{\text{heu}} = 10.0$ , and the bisection iteration

Table I. Simulation benchmark results, reported as averages over 10 runs.

Method	FT (s) $\downarrow$	CR (%) $\uparrow$	OR (%) $\downarrow$	VaE $\uparrow$	CL (ms) $\downarrow$
KW <sup>*</sup>	Colli-Free	<b>73.18</b>	42.52	65.31	20.16 <b>19.47</b>
	Ours	79.80	<b>97.84</b>	<b>1.86</b>	<b>120.33</b> 23.35
TN <sup>†</sup>	Colli-Free	<b>46.66</b>	54.79	68.09	37.47 <b>18.94</b>
	Ours	49.54	<b>95.51</b>	<b>1.00</b>	<b>190.87</b> 27.45
EC <sup>‡</sup>	Colli-Free	<b>149.82</b>	75.56	53.67	23.37 <b>19.33</b>
	Ours	206.64	<b>94.73</b>	<b>0.72</b>	<b>45.51</b> 22.12

\*Kino Wall, <sup>†</sup>Tunnel, <sup>‡</sup>East Church.

limit  $N_{\text{bis}} = 10$ . Each receding-horizon replanning cycle uses a horizon  $\mathcal{H} = 10$  m. We limit the maximum linear/angular velocity as 1.0 m/s and 20°/s in simulation, while 0.5 m/s and 15°/s in real-world flights.

**Baseline.** We compare against prior obstacle-adaptive replanning strategies used in aerial 3D scanning [7], [8]. Since no official open source code is available, we implement them following the original descriptions and denote this baseline as **Colli-Free**, which replans only for collision clearance. For a fair comparison, both our method and **Colli-Free** are integrated into FC-Planner [6] via the proposed plug-in strategy; all other modules are shared, and the only difference lies in the local replanning stage.

**Metrics.** Evaluation focuses on flight efficiency and target visibility. Efficiency is measured by the flight time (FT) to finish the scan, while visibility is quantified by the target coverage rate (CR) that is derived from 3D reconstructions and the occlusion rate (OR), *i.e.*, the fraction of frames where the target is occluded. To intuitively reflect overall scanning quality, we define the visibility-adjusted efficiency (VaE):  $\text{VaE} = \text{CR} \cdot (1 - \text{OR})/\text{FT}$ . We also report the replanning computational latency (CL) to assess real-time responsiveness.

### B. Simulation Evaluations

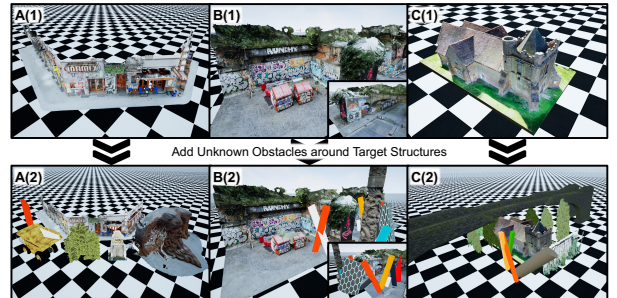


Fig. 5. Simulated scenarios for benchmark experiments.

**Simulated Environments.** To thoroughly validate the performance of our method under diverse conditions, we benchmark it across three challenging simulated scenarios, *Kino Wall* (KW), *Tunnel* (TN), and *East Church* (EC). Before starting the scan, the UAV only has access to the information of target structures (top row in Fig.5) and plans a nominal path accordingly. To emulate unexpected environmental changes, we then add randomly complex obstacles around the target (bottom row in Fig.5), and evaluate different methods' capability to handle them. For each scenario, we run 10 independent trials and report the average results.

**Comparisons and Analysis.** Fig.6 illustrates the full scanning outcome, from trajectories to first-person observations and 3D reconstructions. **Colli-Free** resolves collisions with minimal

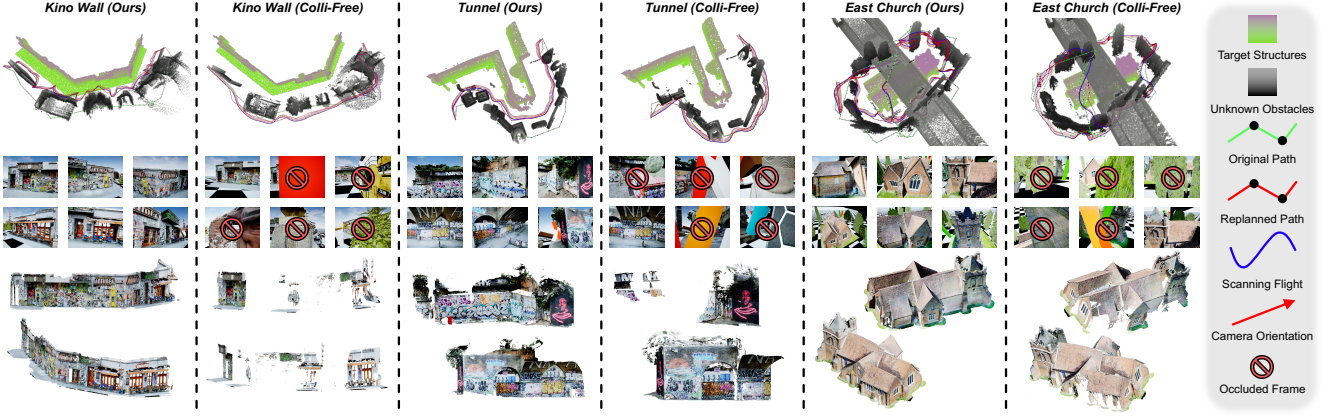


Fig. 6. Comparisons on simulated scenarios. From top to bottom: flight trajectories, onboard first-person-view frames, snapshots of 3D reconstructions.

detours, yet its replanned segments frequently place the FoV behind newly introduced occluders, resulting in long occluded frame sequences and fragmented reconstructions. In contrast, **FC-Vision** explicitly enforces comprehensive and clean sensing during replanning, jointly adjusting position and gimbal attitude to keep the target unobstructed, thereby producing consistently clear frames and substantially more complete reconstructions across all scenarios. Table.I confirms these trends: **FC-Vision** achieves near-complete coverage and reduces occlusions to almost zero, while the flight-time increase remains limited (from +6% to +38% depending on scenario). As a consequence, the scanning quality (VaE) improves by multiple folds. Importantly, this benefit does not come from heavier computation—the replanning latency stays low (CL 22–27 ms), meeting real-time requirements. More details about this experiment can be found in our video.

The key limitation of collision-only consideration lies in treating visibility as an incidental byproduct where occluders are prone to enter the FoV and invalidate a large portion of the scan. On the contrary, **FC-Vision** makes visibility an explicit constraint at both the viewpoint level and the connecting segment level. This turns many failure cases of **Colli-Free** (collision-free but visually blocked) into feasible clean-sensing alternatives with minimal spatial deviation, explaining the substantial reductions in OR and the corresponding multi-fold VaE improvement.

Table II. Comparisons of segment search, reported as averages over 20 runs.

Method	CL (ms) ↓	Length (m) ↓	OR (%) ↓
Corridor	Conv. A* <sup>†</sup>	<b>1.154</b>	<b>39.52</b>
	Our $\Phi$ -A* w/o VC <sup>‡</sup>	3.142	43.26
	Our $\Phi$ -A*	1.269	43.74
Forest	Conv. A* <sup>†</sup>	<b>1.286</b>	<b>49.96</b>
	Our $\Phi$ -A* w/o VC <sup>‡</sup>	3.578	64.39
	Our $\Phi$ -A*	1.453	63.85

<sup>†</sup>Conventional A\*, <sup>‡</sup> $\Phi$ -A\* without visibility cache acceleration.

**Effectiveness of  $\Phi$ -A\*.** To ablate the contribution of our segment search, Table.II and Fig.7 compare  $\Phi$ -A\* with conventional A\* on two representative cases (corridor and forest) over 20 repeated runs. Conventional A\* produces shorter connectors but suffers severe visibility degradation (OR 74.78% and 82.62%), confirming that collision-free navigation alone does not guarantee clean sensing.  $\Phi$ -A\* enforces occlusion-free sensing along the entire segment, achieving OR = 0

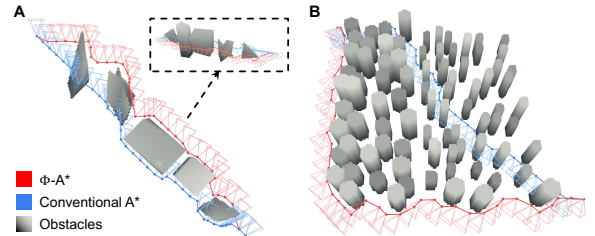


Fig. 7. The qualitative results of  $\Phi$ -A\* vs. conventional A\* in (A) corridor and (B) forest cases.

in both cases at the cost of slightly longer paths, which is expected since visibility constraints restrict feasible passages. Moreover, the proposed visibility cache is critical for real-time performance: it reduces the latency of  $\Phi$ -A\* from 3.14–3.58 ms to 1.27–1.45 ms, approaching conventional A\* while preserving strict visibility guarantees.

### C. Real-world Flight Tests

Table III. Real-world experiments result statistics.

Method	FT (s) ↓	CR (%) ↑	OR (%) ↓	VaE ↑	CL (ms) ↓
RoomRect <sup>*</sup>	Colli-Free	<b>20.42</b>	84.93	73.17	111.59
	Ours	25.13	<b>98.65</b>	<b>0.0</b>	<b>392.56</b>
Room	Colli-Free	<b>133.95</b>	61.23	48.88	23.37
	Ours	167.91	<b>97.36</b>	<b>1.19</b>	<b>57.29</b>

\*Rectangular area.

To further assess the practicality and robustness of our framework, we conduct fully autonomous scanning flights in two indoor real-world sites, *Rectangular Area (Rect.)* and *Room* (Fig.1A and Fig.8A). The experimental protocol mirrors simulation: FC-Planner first generates an initial scanning path from the target structure, after which we insert various objects to alter the environment (Fig.1B and Fig.8B).

Fig.1 and Fig.8 qualitatively demonstrate a significant advantage of **FC-Vision** over the baseline. Although **Colli-Free** remains collision safety, its replanned trajectory often steers the camera towards non-target elements, yielding heavily blocked views and incomplete reconstructions. Conversely, **FC-Vision** proactively routes around online-emerging obstacles and adjusts camera orientation to preserve occlusion-free target observations, resulting in consistently clean frames and substantially more complete surfaces. Table.III corroborates these findings: **FC-Vision** achieves much higher coverage with near-zero occlusion rate, which translates into a large-magnitude gain in the overall task quality (VaE), while incurring only a moderate increase in flight time. Meanwhile, the

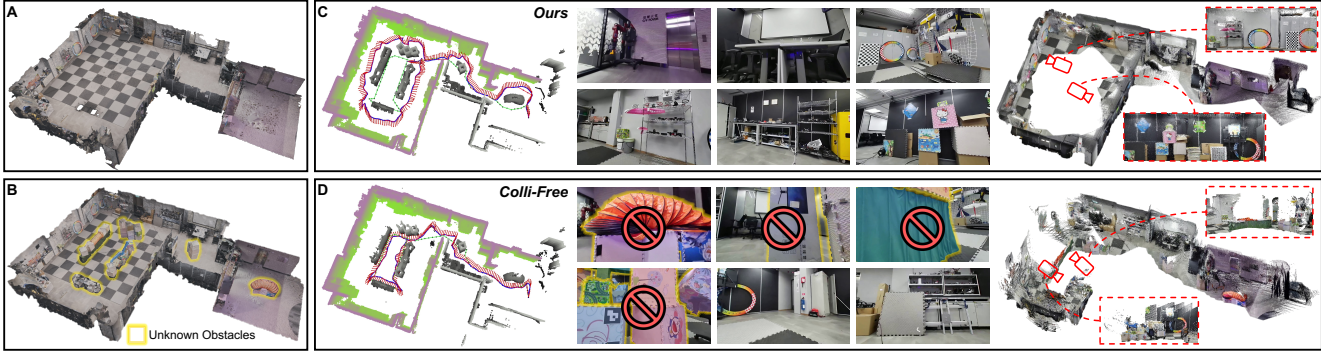


Fig. 8. Real-world test results at the *Room* site. (A) Target structure, (B) Environmental changes: newly introduced unknown obstacles, (C)–(D) Flight trajectories, onboard views, and 3D reconstructions by **FC-Vision** and **Colli-Free**, respectively.

replanning latency stays low on the edge device, confirming its real-time deployability ( $\sim 30$  Hz). These advances stem from our two-level decomposition that turns the otherwise expensive optimization under occlusion-free constraint into several efficiently solvable subproblems, achieving a better balance among safety, efficiency, and target visibility in real flights. Detailed information is provided in our video.

## VII. CONCLUSION

We present **FC-Vision**, a real-time visibility-aware replanning framework empowering occlusion-free and safe aerial scanning of target structure in unknown, cluttered environments. Instead of treating sensing as a byproduct of collision-free navigation, it makes target visibility an explicit constraint and achieves low-latency replanning through a two-level decomposition: (1) an efficient occlusion-free viewpoint repair that preserves intended coverage while minimally deviating from the nominal scan intent; and (2) a clean-sensing segment search in a 5-DoF representation, which enforces consistent FoV-level cleanliness with guaranteed clearance along segments with modest overhead. We further provide a seamless integration strategy that enables plug-in deployment on existing aerial scanning systems. Extensive simulation and real-flight results demonstrate the effectiveness, practicality, and efficiency of our approach. Future work will extend this framework to handle more dynamic scenes and semantic sensing objectives, potentially via end-to-end learning.

## REFERENCES

- [1] D. Lattanzi and G. Miller, “Review of robotic infrastructure inspection systems,” *J. Infrastruct. Syst.*, vol. 23, no. 3, p. 04017004, 2017.
- [2] C. Feng, H. Li, F. Gao, B. Zhou, and S. Shen, “Predrecon: A prediction-boosted planning framework for fast and high-quality autonomous aerial reconstruction,” in *2023 IEEE ICRA*, 2023, pp. 1207–1213.
- [3] A. Bircher, M. Kamel, K. Alexis, M. Burri, P. Oettershagen, S. Omari, T. Mantel, and R. Siegwart, “Three-dimensional coverage path planning via viewpoint resampling and tour optimization for aerial robots,” *AUTON ROBOT*, vol. 40, no. 6, pp. 1059–1078, 2016.
- [4] C. Cao, J. Zhang, M. Travers, and H. Choset, “Hierarchical coverage path planning in complex 3d environments,” in *2020 IEEE ICRA*. IEEE, 2020, pp. 3206–3212.
- [5] Z. Wu, P. Marais, and H. Rüther, “A uav-based sparse viewpoint planning framework for detailed 3d modelling of cultural heritage monuments,” *ISPRS J. Photogramm. Remote Sens.*, vol. 218, pp. 555–571, 2024.
- [6] C. Feng, H. Li, M. Zhang, X. Chen, B. Zhou, and S. Shen, “Fc-planner: A skeleton-guided planning framework for fast aerial coverage of complex 3d scenes,” in *2024 IEEE ICRA*. IEEE, 2024, pp. 8686–8692.
- [7] S. Song, D. Kim, and S. Jo, “Online coverage and inspection planning for 3d modeling,” *AUTON ROBOT*, vol. 44, no. 8, pp. 1431–1450, 2020.
- [8] V. K. Viswanathan, Y. Bai, S. Fredriksson, S. Satpute, C. Kanellakis, and G. Nikolakopoulos, “An adaptive inspection planning approach towards routine monitoring in uncertain environments,” *arXiv preprint arXiv:2510.24554*, 2025.
- [9] B. Zhou, F. Gao, J. Pan, and S. Shen, “Robust real-time uav replanning using guided gradient-based optimization and topological paths,” in *2020 IEEE ICRA*. IEEE, 2020, pp. 1208–1214.
- [10] X. Zhou, Z. Wang, H. Ye, C. Xu, and F. Gao, “Ego-planner: An esdf-free gradient-based local planner for quadrotors,” *IEEE RA-L*, vol. 6, no. 2, pp. 478–485, 2020.
- [11] J. Lu, X. Zhang, H. Shen, L. Xu, and B. Tian, “You only plan once: A learning-based one-stage planner with guidance learning,” *IEEE RA-L*, vol. 9, no. 7, pp. 6083–6090, 2024.
- [12] Z. Zhang and D. Scaramuzza, “Perception-aware receding horizon navigation for mavs,” in *2018 IEEE ICRA*. IEEE, 2018, pp. 2534–2541.
- [13] L. Bartolomei, L. Teixeira, and M. Chli, “Perception-aware path planning for uavs using semantic segmentation,” in *2020 IEEE/RSJ IROS*. IEEE, 2020, pp. 5808–5815.
- [14] Y. Lin, X. Zhang, Y. Liu, D. Wang, and H. Lu, “Gfm-planner: Perception-aware trajectory planning with geometric feature metric,” *arXiv preprint arXiv:2507.16233*, 2025.
- [15] B. Jeon, Y. Lee, and H. J. Kim, “Integrated motion planner for real-time aerial videography with a drone in a dense environment,” in *2020 IEEE ICRA*. IEEE, 2020, pp. 1243–1249.
- [16] J. Ji, N. Pan, C. Xu, and F. Gao, “Elastic tracker: A spatio-temporal trajectory planner for flexible aerial tracking,” in *2022 IEEE ICRA*. IEEE, 2022, pp. 47–53.
- [17] Y. Gao, J. Ji, Q. Wang, R. Jin, Y. Lin, Z. Shang, Y. Cao, S. Shen, C. Xu, and F. Gao, “Adaptive tracking and perching for quadrotor in dynamic scenarios,” *IEEE Transactions on Robotics*, vol. 40, pp. 499–519, 2023.
- [18] W. Jing, J. Polden, W. Lin, and K. Shimada, “Sampling-based view planning for 3d visual coverage task with unmanned aerial vehicle,” in *2016 IEEE/RSJ IROS*. IEEE, 2016, pp. 1808–1815.
- [19] R. Almadhoun, T. Taha, D. Gan, J. Dias, Y. Zweiri, and L. Seneviratne, “Coverage path planning with adaptive viewpoint sampling to construct 3d models of complex structures for the purpose of inspection,” in *2018 IEEE/RSJ IROS*. IEEE, 2018, pp. 7047–7054.
- [20] C. Peng and V. Isler, “Adaptive view planning for aerial 3d reconstruction,” in *2019 IEEE ICRA*. IEEE, 2019, pp. 2981–2987.
- [21] M. De Berg, O. Cheong, M. Van Kreveld, and M. Overmars, *Computational geometry: algorithms and applications*. Springer, 2008.
- [22] C. H. Papadimitriou and K. Steiglitz, *Combinatorial optimization: algorithms and complexity*. Courier Corporation, 1998.
- [23] I. T. Hernádsvölgyi, “Solving the sequential ordering problem with automatically generated lower bounds,” in *Operations Research Proceedings 2003: Selected Papers of the International Conference on Operations Research (OR 2003) Heidelberg, September 3–5, 2003*. Springer, 2004, pp. 355–362.
- [24] C. Feng, G. Zheng, T. Zhuang, Y. Wu, F. He, H. Li, J. Zheng, S. Shen, and B. Zhou, “Flyco: Foundation model-empowered drones for autonomous 3d structure scanning in open-world environments,” *arXiv preprint arXiv:2601.07558*, 2026.
- [25] S. Shah, D. Dey, C. Lovett, and A. Kapoor, “Airsim: High-fidelity visual and physical simulation for autonomous vehicles,” in *Field and service robotics: Results of the 11th international conference*. Springer, 2017, pp. 621–635.